SOLID STATE PHYSICS

Tunable chiral metal organic frameworks toward visible light–driven asymmetric catalysis

Yin Zhang,[1,2]* Jun Guo,[1,2]* Lin Shi,[1] Yanfei Zhu,[1] Ke Hou,[1,2] Yonglong Zheng,[1] Zhiyong Tang[1]†

A simple and effective strategy is developed to realize visible light–driven heterogeneous asymmetric catalysis. A chiral organic molecule, which only has very weak catalytic activity in asymmetric α-alkylation of aldehydes under visible light, is utilized as the ligand to coordinate with different types of metal ions, including Zn^{2+}, Zr^{4+}, and Ti^{4+}, for construction of crystalline metal organic frameworks (MOFs). Impressively, when used as heterogeneous catalysts, all of the synthesized MOFs exhibit markedly enhanced activity. Furthermore, the asymmetric catalytic performance of these MOFs could be easily altered by selecting different metal ions, owing to the tunable electron transfer property between metal ions and chiral ligands. This work will provide a new approach for fabrication of heterogeneous catalysts and trigger more enthusiasm to conduct the asymmetric catalysis driven by visible light.

INTRODUCTION

Asymmetric catalysis is of special interest in biochemistry, medicine, and environmental industry. Typically, heat and light are two major ways to provide the energy for promotion of varied catalytic reactions. Compared with thermal catalysis, photocatalysis (*1*) under solar light is characterized by green, sustainable, and low-cost production; hence, it is always the preferred option for asymmetric catalysis (*2–5*). In 2008, a pioneering work demonstrated visible light–driven asymmetric alkylation of aldehyde with the help of a chiral ligand and Ru(bpy)$_3$$^{2+}$ electron mediator (*6*). Thereafter, a number of homogeneous asymmetric photocatalysis have been successfully implemented by using transition metal (*7–19*) or metal-free organic photosensitizers (*20, 21*), together with different chiral ligands in different systems under visible light irradiation. A significant advance in asymmetric photocatalysis is the combination of photoactive group and chiral center into one molecular catalyst, endowing the advantages of atomically economic structural design, effective photoinduced charge transfer, and convenient separation of products and catalysts. For instance, chiral center, catalytic site, and photoactive core all have been integrated at the iridium atom of a coordination complex to accomplish the photoinduced enantioselective alkylation of acyl imidazole (*22*). Another interesting example is that a chiral amine without a photosensitive group could successfully realize visible light–driven asymmetric alkylation of aldehydes via formation of a transient chiral donor-acceptor complex between catalyst and substrate (*23, 24*).

As for practical application, heterogeneous catalysts have attracted much more interest compared with homogenous ones because of their easy recovery and rapid reuse (*25–30*). Many semiconductors—such as TiO$_2$ (*31–33*), PbBiO$_2$Br (*34*), and Bi$_2$O$_3$ (*35*)—together with a chiral ligand—have been examined in heterogeneous asymmetric photocatalysis. Unfortunately, this heterogeneous catalysis generally could not achieve high stereoselectivity due to difficulties controlling the surface composition and configuration of solid semiconductors. A plausible solution would be the uniform combination of photoactive groups and chiral centers in a porous crystalline material such as

metal organic frameworks (MOFs). However, multifunction in a rigid framework poses a great challenge. Until now, only one study has demonstrated incorporation of three components, namely, zinc ion, stereoselective pyrrolidin-2-ylimidazole, and photoredox 4,4′,4′′-tricarboxytriphenylamine, into an MOF structure to catalyze the asymmetric α-alkylation of aliphatic aldehyde (*36*). Nevertheless, much more work is needed, for instance, design of an organic ligand of both photoactive groups and the chiral center to simplify the preparation process and improve photoactivity efficiency (*37*) as well as exploitation of metal ions interacting organic ligands to further regulate catalytic performance (*38–41*).

Here, a novel strategy is adopted for construction of heterogeneous asymmetric photocatalysis. Chiral photoredox molecules are selected as ligands to coordinate with different metal ions for the formation of MOFs. When these MOFs are used for photocatalytic establishment of a new C–C bond and stereocenter, they exhibit high and adjustable activity that depends on selection of metal ions.

RESULTS AND DISCUSSION

It is clear that the synergistic effect between metal ions and a photoredox chiral ligand is the key to achieving highly efficient asymmetric catalysis (Scheme 1A). First, an organic chiral ligand that contains both a catalytic active site and a visible light absorption group is necessary to conduct photocatalytic asymmetric α-alkylation of aldehydes driven by visible light. Keeping this in mind, we choose N-(tert-butoxycarbonyl)-prolinal (N-Boc-prolinal; II in Scheme 1B), derived from proline, in which a secondary amine group (it is initially protected by a Boc group to prevent deactivation during MOF formation process) activates the aldehyde substrates in an enamine mode, and a formyl group acts as the loop to connect with 2-aminoterephthalic acid (H$_2$BDC-NH$_2$; I in Scheme 1B). The rationale for conjugation with H$_2$BDC-NH$_2$ is two-fold: (i) The carboxylic acid group in H$_2$BDC-NH$_2$ is easy to coordinate with metal ions for MOF construction, and (ii) the phenyl group in H$_2$BDC-NH$_2$ might benefit the separation of photoinduced charge and thus improvement of photocatalytic performance. Scheme 1B outlines the synthetic route of chiral photoredox ligands. S(R)-N-Boc-prolinal (II) was first combined with H$_2$BDC-NH$_2$ (I) through a typical Schiff base condensation (*42*). Afterward, hydrogenation with NaBH$_4$ (*43*) was performed to obtain the amine group–protected molecule [S(R)-Boc-HL; IV] to avoid its unnecessary decomposition during purification and later deprotection process. Many characterizations based on nuclear

[1]Chinese Academy of Science (CAS) Key Laboratory of Nanosystem and Hierarchy Fabrication, CAS Center for Excellence in Nanoscience, National Center for Nanoscience and Technology and University of Chinese Academy of Sciences, Beijing 100190, P. R. China. [2]Center for Nanochemistry, Peking University, Beijing 100871, P. R. China.
*These authors contributed equally to this work.
†Corresponding author. Email: zytang@nanoctr.cn

magnetic resonance (NMR) spectroscopy (figs. S1 to S5) confirm successful synthesis of S(R)-Boc-HL. We intentionally prepared a pure chiral ligand catalyst [S(R)-HL; V] to explore its inherent property toward visible light–driven asymmetric α-alkylation conveniently. Again, the results from NMR (fig. S6) and circular dichroism (CD) spectra (fig. S7) prove the successful preparation of the target S(R)-HL.

Next, three types of metal ions, including Zn^{2+}, Zr^{4+}, and Ti^{4+}, which are well known as metal centers in many MOFs, are used to construct MOFs via coordination with chiral Boc-HL. Fourier transform infrared (FT-IR) spectroscopy data (fig. S8) verify that for-

mation of Boc-MOFs is mainly ascribed to the interaction between metal ions and carboxylic acid groups in S(R)-Boc-HL. Thermogravimetric analysis (TGA) is used to estimate the thermal stability of the Boc-MOFs (fig. S9). Finally, deprotection of Boc groups was carried out by applying a microwave heating method (36, 44) to empty the occupied channels to contact the substrates and recover the amine groups as catalytic centers. The corresponding products are named as Zn-MOF, Zr-MOF, and Ti-MOF. Scanning electron microscopy (SEM) imaging (fig. S10) and N_2 adsorption-desorption measurement are utilized to discern the shape and structure of the prepared catalysts
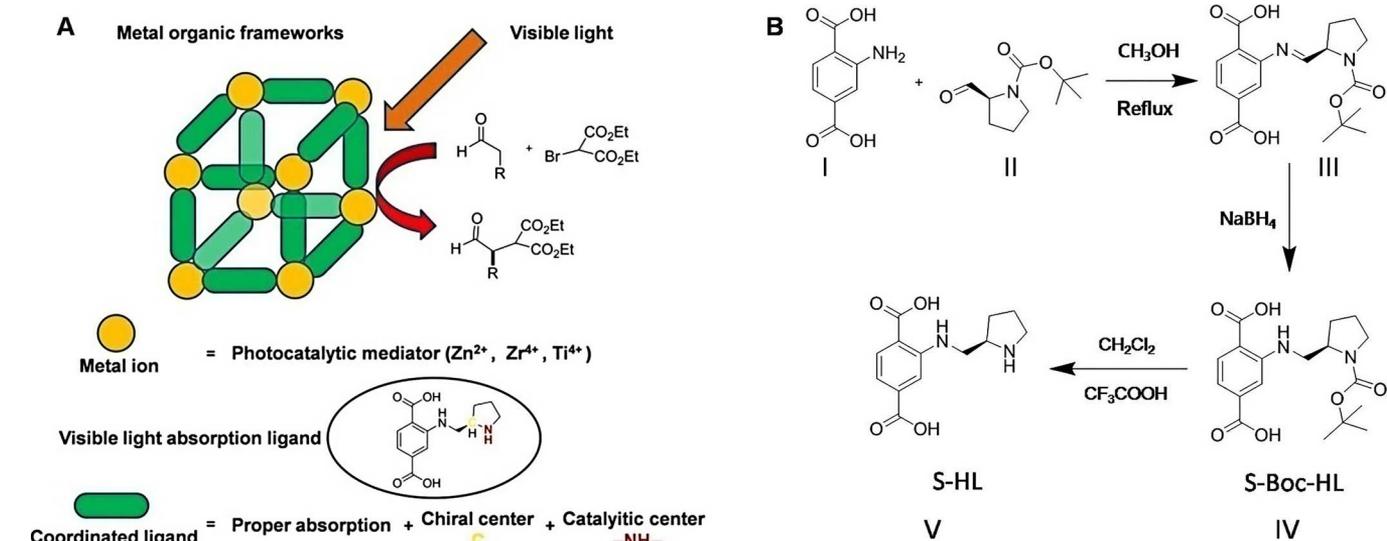
Scheme 1. Basic illustration, ligand design, and synthesis. (**A**) Scheme of photocatalytic asymmetric α-alkylation of aldehyde by MOFs that are constructed with chiral photoredox ligands and metal ions. (**B**) Route to synthesize chiral photoredox ligands.
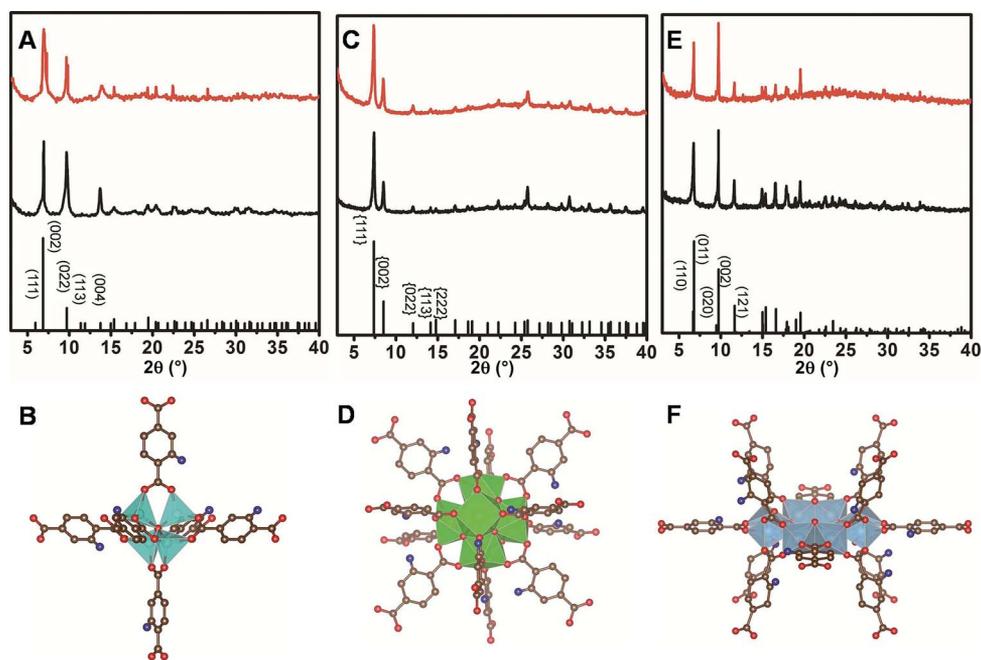

Fig. 1. XRD patterns of crystalline MOFs. (**A** to **F**) Zn-MOF (A), Zr-MOF (C), and Ti-MOF (E) before (black curves) and after (red curves) Boc group removal. Corresponding crystal structures of Zn-MOF (B), Zr-MOF (D), and Ti-MOF (F). In the crystal structures, metal ion is included in the polyhedron, oxygen atom is in red color, carbon atom is in brown color, and the ball in blue color represents a functional group with chiral induction and catalytic ability.

(figs. S11 to S13). Note that FT-IR (fig. S14) analysis manifests successful removal of the Boc groups in MOFs after microwave heating. N_2 adsorption-desorption measurement on all three MOFs further demonstrates the evidently increased surface area and enlarged pore sizes of MOFs after removal of the Boc groups. In detail, the Brunauer-Emmett-Teller surface area and the pore size are 262 m^2/g and 8.5 Å for Zn-MOF, 768 m^2/g and 8.0 Å for Zr-MOF, and 1047 m^2/g and 6 as well as 10 Å for Ti-MOF, which all are large enough to accommodate the substrates for catalysis.

Figure 1 (A, C, and E) presents the powder x-ray diffraction (XRD) patterns of the MOFs before (black curves) and after (red curves) removal of the Boc groups. It is evident that there remains no change in the XRD peaks after microwave heating. This result indicates that the deprotection from Boc-MOFs to MOFs experiences a single-crystal–to–single-crystal transformation without damage of spatial arrangement (44). According to XRD data, the crystal structure of Zn-MOF (Fig. 1A) agrees with that of classic MOF-5 (37), suggesting that Zn_4O clusters are connected orthogonally to six terephthalate units (Fig. 1B). The crystalline nature of Zr-MOF (Fig. 1C) is the same as that of NH_2-UiO-66 (45), and in the cubic framework, $Zr_6O_4(OH)_4$ works as nodes to link with chiral HL ligands (Fig. 1D). Ti-MOF (Fig. 1E) is isostructural to NH_2-MIL-125(Ti) (46), which is built up from the cyclic octamer $Ti_8O_8(OH)_4$ and chiral HL linkers (Fig. 1F).

The colors of MOF products appear different to the naked eye, for instance, yellow brown for Zn-MOF, golden yellow for Zr-MOF, and orange for Ti-MOF powders (fig. S15); thus, qualitative evaluation of their optical absorption properties is performed by ultraviolet-visible (UV-vis) absorption spectroscopy. Compared with the starting material $H_2BDC-NH_2$, the absorption peak of chiral HL is red-shifted from 365 to 382 nm (Fig. 2A), implying more coverage in the visible region. When the chiral ligands are built in MOFs, the absorption peaks display further bathochromic shift to 389, 406, and 420 nm for Zn-MOF, Zr-MOF, and Ti-MOF, respectively (Fig. 2B). Similar red-shift phenomena have been reported in Zn-MOF-5 (47, 48), NH_2-UIO-66 (49), and NH_2-MIL-125(Ti) (50) systems, which are attributed to the ligand-to-metal charge transfer. Notably, different metal ions and ligands have varied interactions and, therefore, distinct optical absorption, endowing us the opportunity to efficiently exploit solar energy via versatile coordination chemistry (51–54).

The CD spectrum of chiral HL (Fig. 2C) exhibits two signals in the range of 200 to 300 nm. The peak at 204 nm is assigned to the transition absorption of the prolinal portion that can be proven by the CD spectrum of original Boc-prolinal (fig. S7B), whereas the other one at 238 nm
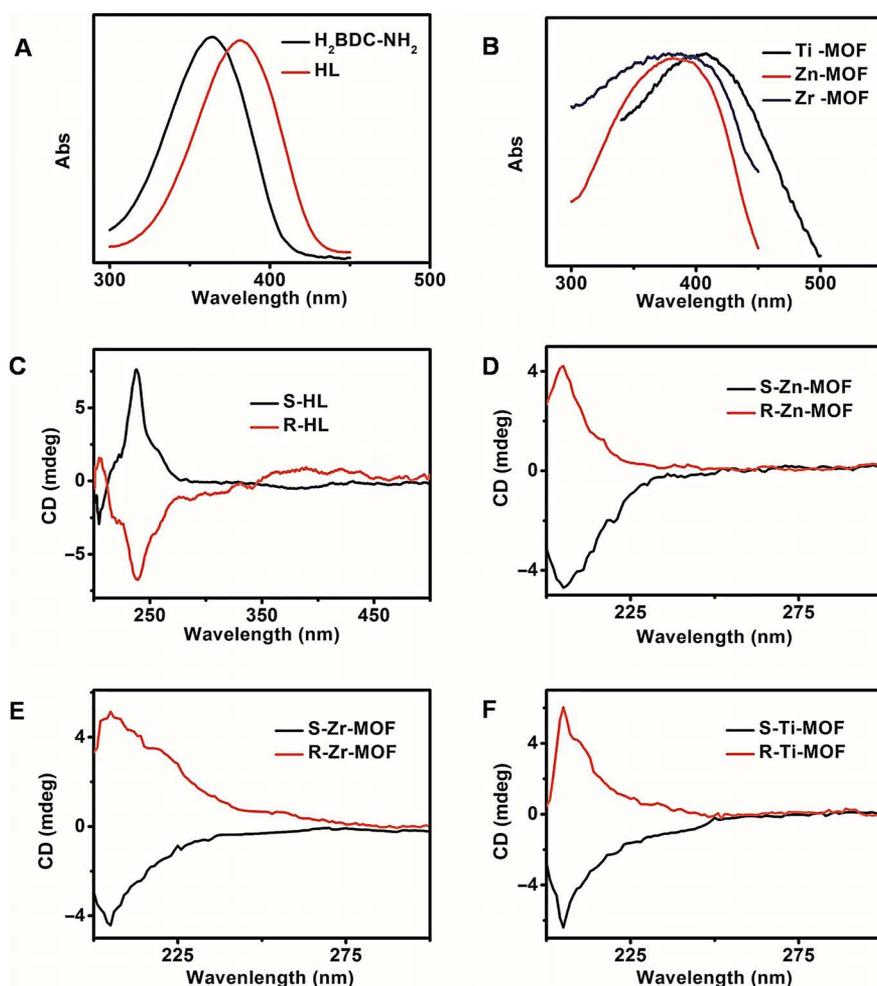

Fig. 2. The light property measurements. (**A**) UV-vis absorption spectra of $H_2BDC-NH_2$ and chiral HL and (**B**) UV-vis absorption spectra of Zn-MOF, Zr-MOF, and Ti-MOF. CD spectra of (**C**) chiral HL, (**D**) Zn MOF, (**E**) Zr-MOF, and (**F**) Ti-MOF.

corresponds to the transition absorption of H_2BDC-NH_2 part (fig. S7C). After incorporation into MOFs, the CD spectra become quite different (Fig. 2, D to F), and only the CD responses of prolinal parts remain. Together, the CD observation confirms the maintenance of chirality inside MOF products.

The photocatalytic activity of all of the synthesized MOFs is assessed by the reactions of asymmetric C–C bond formation via α-alkylation of aldehydes under visible light irradiation (figs. S16 to S31). Table 1 summarizes the experimental results, from which several conclusions are drawn: (i) The S(R)-HL itself has rather weak catalytic activity under visible light (entries 1 to 4). When the S(R)-HL is used in the reaction, irradiation under high-energy light (200 W) affords a moderate conversion of 55% and an enantiomeric excess (ee) value of 74%, whereas less than 10% conversion is obtained when a 25-W output is adopted as the light source, which should be caused by the poor light absorption of chiral HL in the visible region. A similar result was reported (6) that a rather high conversion efficiency was obtained in the absence of

$Ru(bpy)_3^{2+}$ light sensitizers when a high-energy UV irradiation (300 to 350 nm) was used. (ii) All the S(R)-Zn-MOF, S(R)-Zr-MOF, and S(R)-Ti-MOF exhibit markedly improved catalytic performance at 25-W illumination compared with chiral HL (entries 5 to 10). Furthermore, different MOF catalysts have distinct photocatalytic activity. It is reported that as a semiconductor, Zn-MOF-5 undergoes charge separation at a microsecond scale upon light excitation (37). However, the absorption of Zn-MOF in the visible portion is still small when irradiated by 25-W visible light, causing a rather low conversion of 40% and an ee value of 55% (entries 5 to 6). NH_2-MIL-125(Ti) is the most studied MOF (55–57) in the photocatalysis with visible light. It is known that the highest occupied crystal orbital (HOCO) of the Ti-MOF is localized at the organic linker, and the lowest unoccupied crystalline orbital (LOCO) is centered at Ti d-orbital to meet the spatial and energetic requirements, allowing for an efficient overlap. Ti^{3+} species are easily formed upon irradiation by visible light, thus promoting a long-lived ligand-to-metal charge transfer (50). Because of these characteristics, the chiral Ti-MOF shows almost 100% conversion and a high 85% ee value under 25-W visible illumination (entries 9 to 10). In regard to chiral Zr-MOFs, a conversion of 46% and an ee value of 64% are obtained (entries 7 to 8). As for NH_2-UiO-66 with an optical bandgap of 2.75 eV, the photoinduced electrons by visible light could cause generation of Zr^{3+} species via charge transfer from the excited ligand to Zr oxo clusters, but the d-orbitals in Zr are too low in binding energy and thus cannot overlap with the π* orbital of the ligand effectively, making both frontier orbitals localized more at the organic linker (58, 59). In general, the excitons in organic molecules are relatively short-lived, which result in lower catalytic activity. As a result, Zr-MOF displays better catalytic performance than Zn-MOF but much lower efficiency than Ti-MOF under similar visible light illumination. (iii) Comparative experiments indicate that the chiral catalytic reactions do not happen without visible light (entry 14, Table 1) or catalysts (entry 15). In addition, these reactions cannot occur with Boc-MOFs as catalysts due to the blockage of catalytically active amine groups (table S2). Among the tested solvents, dimethylformamide (DMF) is the best choice to achieve both high conversion efficiency and marked ee value (entries 12 to 13), which is reasonable considering that the photoredox potentials vary with different solvents (20). In addition, temperature has the influence on photocatalytic performance; for example, low temperature decreases the activity of Ti-MOF but raises the stereoselectivity (entry 11). (iv) The MOF heterogeneous catalysts demonstrate excellent stability and reusability, for instance, their crystalline structure and catalytic performance are well retained after three photocatalytic cycles (table S3 and fig. S31). (v) These novel MOFs show universality in asymmetric photocatalysis. As an example, good conversion and enantiomeric excess are achieved when another substrate cis-6-nonenal is used with S(R)-Ti-MOF (entries 16 to 17).

With the above facts, one can deduce that the photoinduced charge separation determines the catalytic efficiency of MOFs. First, substrate aldehyde diffuses into the cavities of MOFs, inside which aldehyde condenses with the amine group of a chiral ligand to form the enamine intermediate that is confirmed by FT-IR spectra (fig. S32) (6). Next, the chiral MOFs would accept a photon from a light source and cause charge separation, where the hole is located at the HOCO, and the electron reduces the metal ions (37, 51–54, 58, 59). Then, the electron is further transferred to the diethyl bromomalonate (fig. S35), resulting in recovery of metal ion, loss of bromide anion, and generation of α-carbonyl radical (36). Afterward, the α-carbonyl radical adds to the enamine to form an α-radical intermediate rapidly (6, 36). Finally,

Table 1. Catalytic performance under different conditions. THF, tetrahydrofuran.

Entry	Output (W)	Catalyst	Temperature (°C)	Solvent	Conversion (%)	ee (%)
Substrate: 3-phenylpropionaldehyde*						
1	200[†]	S-HL	0	DMF	50	+78
2	200	R-HL	20	DMF	52	−72
3	200	S-HL	20	DMF	55	+74
4	25	S-HL	20	DMF	8	nd[‡]
5	25	S-Zn-MOF	20	DMF	40	+55
6	25	R-Zn-MOF	20	DMF	38	−53
7	25	S-Zr-MOF	20	DMF	46	+64
8	25	R-Zr-MOF	20	DMF	47	−66
9	25	S-Ti-MOF	20	DMF	95	+84
10	25	R-Ti-MOF	20	DMF	98	−85
11	25	S-Ti-MOF	0	DMF	90	+87
12	25	S-Ti-MOF	20	THF	21	+45
13	25	S-Ti-MOF	20	CH_3CN	43	+56
14	—	S-Ti-MOF	20	DMF	5	nd
15	25	—	20	DMF	0	nd
Substrate: cis-6-nonenal*						
16	25	S-Ti-MOF	20	DMF	97	+85
17	25	R-Ti-MOF	20	DMF	98	−84

*Catalytic condition: catalyst (0.025 mmol, 0.05 equiv), alkyl bromide (0.5 mmol, 1 equiv), aldehyde (1.0 mmol, 2 equiv), 2,6-lutidine (1.0 mmol, 2 equiv), and solvent (1 ml) under light irradiation for 20 hours. Light source was 8 cm away from the reaction vessel. †Light source used in all reaction was an output tunable xenon lamp housed with a filter to cut off the light at <400 nm. ‡nd, not detected; ee value was tested following the reported method.

the α-radical intermediate is oxidized by the hole located at HOCO, yielding the iminium ion that releases product and catalyst (33–35) into the next cycle via hydrolysis (scheme S3).

CONCLUSIONS

In conclusion, a new type of organic ligand integrated with chiral center and photoredox property is designed and synthesized successfully, which is further coordinated with different metal ions to construct chiral MOFs. When used as catalysts, these MOFs exhibit significantly improved conversion and stereoselectivity in asymmetric α-alkylation of aldehydes under visible light. Notably, photocatalytic performance can be tailored by using MOFs with varied metal ions. Detailed experimental observations and mechanistic investigations reveal that differences in optical absorption and charge separation among MOFs are the key to determining the photocatalytic performance. Our findings open a pathway for preparation of cheap but high-performance photocatalysts toward heterogeneous asymmetric catalysis.

MATERIALS AND METHODS
Standard photocatalytic operation

First, catalysts were weighed and added to a photoreaction vessel (10 ml) that was wholly wrapped with aluminum foil. To exclude the influence of oxygen, the vessel was then transferred into N_2-fulfilled glove box. Subsequently, liquid substrates and 1 ml of anhydrous DMF were added and mixed thoroughly under magnetic stirring. Afterward, the vessel was sealed with a latex plug and transferred into a photoreaction box, where a light source and a magnetic stirrer were kept inside (fig. S16). To keep the temperature constant (20°C), the vessel was connected to a circulating condensation system during the whole reaction. Aluminum foil was then stripped off, and the reaction was initiated by turning on the lamp source. After stirring for 20 hours, the mixture was taken out and centrifuged at 10,000 rpm on a centrifuge for 5 min. After centrifugation, the remaining solids were washed twice with 2 ml of DMF and dried in a vacuum oven at 40°C before reuse; meanwhile, 10 μl of supernatant solution sample was injected into gas chromatography/mass spectrometry (GC-MS) to evaluate the conversion, and the remaining solution was concentrated in the vacuum oven. The obtained oil-like raw product was further purified by column chromatography using hexane/ethyl acetate as the eluent. Finally, ^{1}H NMR was used to determine the ee value by following the reported general method (6).

Catalytic performance evaluation methods
Conversion ratio

The obtained supernatant was directly injected into GC-MS, and the result was calculated on the basis of the relative conversion ratio of diethyl bromomalonate because the aldehyde substrate was excessive. On the other hand, the absolute conversion value was obtained by separating the target products from the resultant supernatant using the column chromatography method. These two values are very close, and for simplification, all of the conversion ratios listed in Table 1 were calculated on the basis of GC-MS results. The experimental GC-MS condition was summarized as follows: The temperature of oven was kept at 50°C for 1 min and then increased to 220°C with a heating speed of 10°C/min, followed by a stay for 2 min. Capillary column was kept in He gas atmosphere all the time. The ionization source was electron ionization.

ee value

^{1}H NMR was used to determine the ee value following a reported general method (6). Twenty milligrams of purified aldehyde product was added to a mixture of 8.5 mg (2S,4S)-(+)-pentanediol (>99% ee) and 1.5 mg of p-toluenesulfonic acid hydrate in CH_2Cl_2 (1 ml). The aldehyde product would react with pentanediol to generate diastereomeric acetals in the mixture, which was then concentrated in vacuum. After ascertaining complete consumption of the aldehyde (as judged by thin-layer chromatography analysis), the ee value of the as-formed diastereomeric acetals was determined by integration of two ^{1}H NMR signals (both doublets) in $CDCl_3$.

SUPPLEMENTARY MATERIALS

REFERENCES AND NOTES

1. B. König, *Chemical Photocatalysis* (De Gruyter, 2013), pp. 1–376.
2. P. Melchiorre, Light in aminocatalysis: The asymmetric intermolecular α-alkylation of aldehydes. *Angew. Chem. Int. Ed.* **48**, 1360–1363 (2009).
3. R. Brimioulle, D. Lenhart, M. M. Maturi, T. Bach, Enantioselective catalysis of photochemical reactions. *Angew. Chem. Int. Ed.* **54**, 3872–3890 (2015).
4. E. Meggers, Asymmetric catalysis activated by visible light. *Chem. Commun.* **51**, 3290–3301 (2015).
5. C. Wang, Z. Lu, Catalytic enantioselective organic transformations via visible light photocatalysis. *Org. Chem. Front.* **2**, 179–190 (2015).
6. D. A. Nicewicz, D. W. C. MacMillan, Merging photoredox catalysis with organocatalysis: The direct asymmetric alkylation of aldehydes. *Science* **322**, 77–80 (2008).
7. D. A. DiRocco, T. Rovis, Catalytic asymmetric α-acylation of tertiary amines mediated by a dual catalysis mode: N-heterocyclic carbene and photoredox catalysis. *J. Am. Chem. Soc.* **134**, 8094–8097 (2012).
8. J. Du, K. L. Skubi, D. M. Schultz, T. P. Yoon, A dual-catalysis approach to enantioselective [2 + 2] photocycloadditions using visible light. *Science* **344**, 392–396 (2014).
9. Y. Zhu, L. Zhang, S. Luo, Asymmetric α-photoalkylation of β-ketocarbonyls by primary amine catalysis: Facile access to acyclic all-carbon quaternary stereocenters. *J. Am. Chem. Soc.* **136**, 14642–14645 (2014).
10. L. Ruiz Espelt, I. S. McPherson, E. M. Wiensch, T. P. Yoon, Enantioselective conjugate additions of α-amino radicals via cooperative photoredox and Lewis acid catalysis. *J. Am. Chem. Soc.* **137**, 2452–2455 (2015).
11. E. R. Welin, A. A. Warkentin, J. C. Conrad, D. W. C. MacMillan, Enantioselective α-alkylation of aldehydes by photoredox organocatalysis: Rapid access to pharmacophore fragments from β-cyanoaldehydes. *Angew. Chem. Int. Ed.* **54**, 9668–9672 (2015).
12. D. A. Nagib, M. E. Scott, D. W. C. MacMillan, Enantioselective α-trifluoromethylation of aldehydes via photoredox organocatalysis. *J. Am. Chem. Soc.* **131**, 10875–10877 (2009).
13. H.-W. Shih, M. N. Vander Wal, R. L. Grange, D. W. C. MacMillan, Enantioselective α-benzylation of aldehydes via photoredox organocatalysis. *J. Am. Chem. Soc.* **132**, 13600–13603 (2010).
14. L. J. Rono, H. G. Yayla, D. Y. Wang, M. F. Armstrong, R. R. Knowles, Enantioselective photoredox catalysis enabled by proton-coupled electron transfer: Development of an asymmetric aza-pinacol cyclization. *J. Am. Chem. Soc.* **135**, 17735–17738 (2013).
15. J. A. Terrett, M. D. Clift, D. W. C. MacMillan, Direct β-alkylation of aldehydes via photoredox organocatalysis. *J. Am. Chem. Soc.* **136**, 6858–6861 (2014).
16. D. Uraguchi, N. Kinoshita, T. Kizu, T. Ooi, Synergistic catalysis of ionic brønsted acid and photosensitizer for a redox neutral asymmetric α-coupling of N-arylaminomethanes with aldimines. *J. Am. Chem. Soc.* **137**, 13768–13771 (2015).
17. A. Gualandi, M. Marchini, L. Mengozzi, M. Natali, M. Lucarini, P. Ceroni, P. G. Cozzi, Organocatalytic enantioselective alkylation of aldehydes with [Fe(bpy)₃]Br₂ catalyst and visible light. *ACS Catal.* **5**, 5927–5931 (2015).
18. Z. Zuo, H. Cong, W. Li, J. Choi, G. C. Fu, D. W. C. MacMillan, Enantioselective decarboxylative arylation of α-amino acids via the merger of photoredox and nickel catalysis. *J. Am. Chem. Soc.* **138**, 1832–1835 (2016).
19. Q. M. Kainz, C. D. Matier, A. Bartoszewicz, S. L. Zultanski, J. C. Peters, G. C. Fu, Asymmetric copper-catalyzed C-N cross-couplings induced by visible light. *Science* **351**, 681–684 (2016).
20. M. Neumann, S. Füldner, B. König, K. Zeitler, Metal-free, cooperative asymmetric organophotoredox catalysis with visible light. *Angew. Chem. Int. Ed.* **50**, 951–954 (2011).
21. K. Fidaly, C. Ceballos, A. Falguières, M. S.-I. Veitia, A. Guy, C. Ferroud, Visible light photoredox organocatalysis: A fully transition metal-free direct asymmetric α-alkylation of aldehydes. *Green Chem.* **14**, 1293–1297 (2012).
22. H. Huo, X. Shen, C. Wang, L. Zhang, P. Röse, L.-A. Chen, K. Harms, M. Marsch, G. Hilt, E. Meggers, Asymmetric photoredox transition-metal catalysis activated by visible light. *Nature* **515**, 100–103 (2014).
23. E. Arceo, I. D. Jurberg, A. Álvarez-Fernández, P. Melchiorre, Photochemical activity of a key donor-acceptor complex can drive stereoselective catalytic α-alkylation of aldehydes. *Nat. Chem.* **5**, 750–756 (2013).
24. M. Silvi, E. Arceo, I. D. Jurberg, C. Cassani, P. Melchiorre, Enantioselective organocatalytic alkylation of aldehydes and enals driven by the direct photoexcitation of enamines. *J. Am. Chem. Soc.* **137**, 6120–6123 (2015).
25. F.-X. Xiao, J. Miao, B. Liu, Layer-by-layer self-assembly of CdS quantum dots/graphene nanosheets hybrid films for photoelectrochemical and photocatalytic applications. *J. Am. Chem. Soc.* **136**, 1559–1569 (2014).
26. W. Wang, Y. Ye, J. Feng, M. Chi, J. Guo, Y. Yin, Enhanced photoreversible color switching of redox dyes catalyzed by barium-doped TiO₂ nanocrystals. *Angew. Chem. Int. Ed.* **54**, 1321–1326 (2015).
27. S. Liu, J. Zhang, R. Dong, P. Gordiichuk, T. Zhang, X. Zhuang, Y. Mai, F. Liu, A. Herrmann, X. Feng, Two-dimensional mesoscale-ordered conducting polymers. *Angew. Chem. Int. Ed.* **55**, 12516–12521 (2016).
28. B. Luo, G. Liu, L. Wang, Recent advances in 2D materials for photocatalysis. *Nanoscale* **8**, 6904–6920 (2016).
29. Y. Cao, W. Geng, R. Shi, L. Shang, G. I. N. Waterhouse, L. Liu, L.-Z. Wu, C.-H. Tung, Y. Yin, T. Zhang, Thiolate-mediated photoinduced synthesis of ultrafine Ag₂S quantum dots from silver nanoparticles. *Angew. Chem. Int. Ed.* **55**, 14952–14957 (2016).
30. F.-K. Shieh, S.-C. Wang, C.-I. Yen, C.-C. Wu, S. Dutta, L.-Y. Chou, J. V. Morabito, P. Hu, M.-H. Hsu, K. C.-W. Wu, C.-K. Tsung, Imparting functionality to biocatalysts via embedding enzymes into nanoporous materials by a de novo approach: Size-selective sheltering of catalase in metal–organic framework microcrystals. *J. Am. Chem. Soc.* **13**, 4276–4279 (2015).
31. X.-H. Ho, M.-J. Kang, S.-J. Kim, E. D. Park, H.-Y. Jang, Green organophotocatalysis. TiO₂-induced enantioselective α-oxyamination of aldehydes. *Catal. Sci. Technol.* **1**, 923–926 (2011).
32. H.-S. Yoon, X.-H. Ho, J. Jang, H.-J. Lee, S.-J. Kim, H.-Y. Jang, N719 dye-sensitized organophotocatalysis: Enantioselective tandem Michael addition/oxyamination of aldehydes. *Org. Lett.* **14**, 3272–3275 (2012).
33. M. Cherevatskaya, M. Neumann, S. Füldner, C. Harlander, S. Kümmel, S. Dankesreiter, A. Pfitzner, K. Zeitler, B. König, Visible-light-promoted stereoselective alkylation by combining heterogeneous photocatalysis with organocatalysis. *Angew. Chem. Int. Ed.* **51**, 4062–4066 (2012).
34. X. Li, J. Wang, D. Xu, Z. Sun, Q. Zhao, W. Peng, Y. Li, G. Zhang, F. Zhang, X. Fan, NbSe₂ nanosheet supported PbBiO₂Br as a high performance photocatalyst for the visible light-driven asymmetric alkylation of aldehyde. *ACS Sustainable Chem. Eng.* **3**, 1017–1022 (2015).
35. P. Riente, A. Matas Adams, J. Albero, E. Palomares, M. A. Pericàs, Light-driven organocatalysis using inexpensive, notoxic Bi₂O₃ as the photocatalyst. *Angew. Chem. Int. Ed.* **53**, 9613–9616 (2014).
36. P. Wu, C. He, J. Wang, X. Peng, X. Li, Y. An, C. Duan, Photoactive chiral metal–organic frameworks for light-driven asymmetric α-alkylation of aldehydes. *J. Am. Chem. Soc.* **134**, 14991–14999 (2012).
37. M. Alvaro, E. Carbonell, B. Ferrer, F. X. Llabrés i Xamena, H. Garcia, Semiconductor behavior of a metal-organic framework (MOF). *Chemistry* **13**, 5106–5112 (2007).
38. C. G. Silva, A. Corma, H. García, Metal–organic frameworks as semiconductors. *J. Mater. Chem.* **20**, 3141–3156 (2010).
39. T. Zhang, W. Lin, Metal–organic frameworks for artificial photosynthesis and photocatalysis. *Chem. Soc. Rev.* **43**, 5982–5993 (2014).
40. D. M. D'Alessandro, Exploiting redox activity in metal–organic frameworks: Concepts, trends and perspectives. *Chem. Commun.* **52**, 8957–8971 (2016).
41. A. Dhakshinamoorthy, A. M. Asiri, H. García, Metal-organic framework (MOF) compounds: Photocatalysts for redox reactions and solar fuel production. *Angew. Chem. Int. Ed.* **55**, 5414–5445 (2016).
42. A. Sasmal, S. Saha, C. J. Gómez-García, C. Desplanches, E. Garribba, A. Bauzá, A. Frontera, R. Scott, R. J. Butcher, S. Mitra, Reversible switching of the electronic ground state in a pentacoordinated Cu(II) complex. *Chem. Commun.* **49**, 7806–7808 (2013).
43. T. Kundu, S. C. Sahoo, R. Banerjee, Relating pore hydrophilicity with vapour adsorption capacity in a series of amino acid based metal organic frameworks. *CrstEngComm* **15**, 9634–9640 (2013).
44. D. J. Lun, G. I. N. Waterhouse, S. G. Telfer, A general thermolabile protecting group strategy for organocatalytic metal–organic frameworks. *J. Am. Chem. Soc.* **133**, 5806–5809 (2011).
45. M. J. Katz, Z. J. Brown, Y. J. Colón, P. W. Siu, K. A. Scheidt, R. Q. Snurr, J. T. Hupp, O. K. Farha, A facile synthesis of UiO-66, UiO-67 and their derivatives. *Chem. Commun.* **49**, 9449–9451 (2013).
46. S.-N. Kim, J. Kim, H.-Y. Kim, H.-Y. Cho, W.-S. Ahn, Adsorption/catalytic properties of MIL-125 and NH₂-MIL-125. *Catal. Today* **204**, 85–93 (2013).
47. J. H. Choi, Y. J. Choi, J. W. Lee, W. H. Shin, J. K. Kang, Tunability of electronic band gaps from semiconducting to metallic states via tailoring Zn ions in MOFs with Co ions. *Phys. Chem. Chem. Phys.* **11**, 628–631 (2009).
48. M. C. Das, H. Xu, Z. Wang, G. Srinivas, W. Zhou, Y.-F. Yue, V. N. Nesterov, G. Qian, B. Chen, A Zn₄O-containing doubly interpenetrated porous metal–organic frameworks for photocatalytic decomposition of methyl orange. *Chem. Commun.* **47**, 11715–11717 (2011).
49. K. Hendrickx, D. E. P. Vanpoucke, K. Leus, K. Lejaeghere, A. Van Yperen-De Deyne, V. Van Speybroeck, P. Van Der Voort, K. Hemelsoet, Understanding intrinsic light absorption properties of UiO-66 frameworks: A combined theoretical and experimental study. *Inorg. Chem.* **54**, 10701–10710 (2015).
50. M. A. Nasalevich, C. H. Hendon, J. G. Santaclara, K. Svane, B. van der Linden, S. L. Veber, M. V. Fedin, A. J. Houtepen, M. A. van der Veen, F. Kapteijn, A. Walsh, J. Gascon, Electronic origins of photocatalytic activity in d⁰ metal organic frameworks. *Sci. Rep.* **6**, 23676 (2016).
51. C.-K. Lin, D. Zhao, W.-Y. Gao, Z. Yang, J. Ye, T. Xu, Q. Ge, S. Ma, D.-J. Liu, Tunability of band gaps in metal–organic frameworks. *Inorg. Chem.* **51**, 9039–9044 (2012).
52. C. H. Hendon, D. Tiana, M. Fontecave, C. Sanchez, L. D'Arras, C. Sassoye, L. Rozes, C. Mellot-Draznieks, A. Walsh, Engineering the optical response of the titanium-MIL-125

metal–organic framework through ligand functionalization. *J. Am. Chem. Soc.* **135**, 10942–10945 (2013).

53. T. L. H. Doan, H. L. Nguyen, H. Q. Pham, N.-N. Pham-Tran, T. N. Le, K. E. Cordova, Tailoring the optical absorption of water-stable Zr^{IV}- and Hf^{IV}-based metal–organic framework photocatalysts. *Chem. Asian J.* **10**, 2660–2668 (2015).

54. S. Pu, L. Xu, L. Sun, H. Du, Tuning the optical properties of the zirconium–UiO-66 metal–organic framework for photocatalytic degradation of methyl orange. *Inorg. Chem. Commun.* **52**, 50–52 (2015).

55. Y. Horiuchi, T. Toyao, M. Saito, K. Mochizuki, M. Iwata, H. Higashimura, M. Anpo, M. Matsuoka, Visible-light-promoted photocatalytic hydrogen production by using an amino-functionalized Ti(IV) metal–organic framework. *J. Phys. Chem. C* **116**, 20848–20853 (2012).

56. M. de Miguel, F. Ragon, T. Devic, C. Serre, P. Horcajada, H. García, Evidence of photoinduced charge separation in the metal–organic framework MIL-125(Ti)-NH$_2$. *ChemPhysChem* **13**, 3651–3654 (2012).

57. J. Gao, J. Miao, P.-Z. Li, W. Y. Teng, L. Yang, Y. Zhao, B. Liu, Q. Zhang, A p-type Ti(IV)-based metal–organic framework with visible-light photo-response. *Chem. Commun.* **50**, 3786–3788 (2014).

58. J. Long, S. Wang, Z. Ding, S. Wang, Y. Zhou, L. Huang, X. Wang, Amine-functionalized zirconium metal–organic framework as efficient visible-light photocatalyst for aerobic organic transformations. *Chem. Commun.* **48**, 11656–11658 (2012).

59. D. Sun, Y. Fu, W. Liu, L. Ye, D. Wang, L. Yang, X. Fu, Z. Li, Studies on photocatalytic CO$_2$ reduction over NH$_2$-UiO-66(Zr) and its derivatives: Towards a better understanding of photocatalysis on metal–organic frameworks. *Chem. Eur. J.* **19**, 14279–14285 (2013).

60. J. Hafizovic, M. Bjørgen, U. Olsbye, P. D. C. Dietrel, S. Bordiga, C. Prestipino, C. Lamberti, K. P. Lillerud, The inconsistency in adsorption properties and powder XRD data of MOF-5 is rationalized by framework interpenetration and the presence of organic and inorganic species in the nanocavities. *J. Am. Chem. Soc.* **129**, 3612–3620 (2007).

61. R. K. Deshpande, J. L. Minnaar, S. G. Telfer, Thermolabile groups in metal-organic frameworks: Suppression of network interpenetration, post-synthetic cavity expansion, and protection of reactive functional groups. *Angew. Chem. Int. Ed.* **49**, 4598–4602 (2010).

62. S. Han, Y. Wei, C. Valente, I. Lagzi, J. J. Gassensmith, A. Coskun, J. F. Stoddart, B. A. Grzybowski, Chromatography in a single metal–organic framework (MOF) crystal. *J. Am. Chem. Soc.* **132**, 16358–16361 (2010).

63. Y. Fu, D. Sun, Y. Chen, R. Huang, Z. Ding, X. Fu, Z. Li, An amine-functionalized titanium metal-organic framework photocatalyst with visible-light-induced activity for CO$_2$ reduction. *Angew. Chem. Int. Ed.* **51**, 3364–3367 (2012).

64. D. Sun, W. Liu, Y. Fu, Z. Fang, F. Sun, X. Fu, Y. Zhang, Z. Li, Noble metals can have different effects on photocatalysis over metal-organic frameworks (MOFs): A case study on M/NH$_2$-MIL-125(Ti) (M=Pt and Au). *Chemistry* **20**, 4780–4788 (2014).

65. D. D. Tanner, H. K. Singh, Reduction of α-halo ketones by organotin hydrides. An electron-transfer-hydrogen atom abstraction mechanism. *J. Org. Chem.* **51**, 5182–5186 (1986).

66. B. Li, J. Liu, Z. Nie, W. Wang, D. Reed, J. Liu, P. McGrail, V. Sprenkle, Metal–organic frameworks as highly active electrocatalysts for high-energy density, aqueous zinc-polyiodide redox flow batteries. *Nano Lett.* **16**, 4335–4340 (2016).

Citation: Y. Zhang, J. Guo, L. Shi, Y. Zhu, K. Hou, Y. Zheng, Z. Tang, Tunable chiral metal organic frameworks toward visible light–driven asymmetric catalysis. *Sci. Adv.* **3**, e1701162 (2017).

Science Advances

Tunable chiral metal organic frameworks toward visible light–driven asymmetric catalysis

Yin Zhang, Jun Guo, Lin Shi, Yanfei Zhu, Ke Hou, Yonglong Zheng and Zhiyong Tang

ARTICLE TOOLS	http://advances.sciencemag.org/content/3/8/e1701162
SUPPLEMENTARY MATERIALS	http://advances.sciencemag.org/content/suppl/2017/08/14/3.8.e1701162.DC1
REFERENCES	This article cites 65 articles, 3 of which you can access for free http://advances.sciencemag.org/content/3/8/e1701162#BIBL
PERMISSIONS	http://www.sciencemag.org/help/reprints-and-permissions

Use of this article is subject to the Terms of Service